1-1-1980

Computer-Aided Design of Optimal Infrared Detector Preamplifiers

D. Gary Frodsham

Doran J. Baker

Frodsham, D. Gary, and Doran J. Baker. 1980. "Computer-Aided Design of Optimal Infrared Detector Preamplifiers." *Proceedings of SPIE* 0246: 39–47. doi:10.1117/12.959354.

Computer-aided design of optimal infrared detector preamplifiers

D. Gary Frodsham, Doran J. Baker
Electro-Dynamics Laboratories, Department of Electrical Engineering
Utah State University, UMC 41, Logan, UT 84322

Abstract

A mathematical model is given for a frequency-compensated detector/preamplifier appropriate for cryogenically-cooled infrared sensors operating under low background conditions. By use of a digital computer, this model is used to rapidly select the optimal combination of design values. These parameters include load resistance, compensation resistance, compensation capacitance, chopping frequency and detector area to meet desired specifications of noise equivalent power, frequency response, dynamic range, and level of output noise. This computer-aided optimal design approach is demonstrated using a contemporary infrared sensor application.

Introduction

The optimal design of infrared detector/preamplifier configurations is complicated by nonlinear interdependencies among system characteristic factors including the frequency response, the dynamic range, the output noise level, the detector size and the noise equivalent power of the sensor. The calculation and plotting of the interactive effects due to varying design parameters is arduous. However, the advent of the desk-top computer-graphic system has greatly facilitated the optimization procedure. Once the software has been developed, the engineer can in a matter of a few minutes plot a family of curves of NEP as a function of load resistance, frequency or detector size, for example.

The mathematical model given in this paper is an expansion of the work previously reported by Frodsham and Baker.[1] The algorithms are limited to detector/preamplifier configurations operating under low infrared background (zilch) and white input noise conditions. However, the algorithms have proven to be sufficiently accurate for the designer in characterizing most contemporary cryogenically-cooled detectors combined with JFET input electrometer preamplifiers.

Detector/preamplifier configuration

The infrared detector and preamplifier combination with frequency compensation is illustrated in Figure 1. The negative feedback elements of the operational preamplifier of open loop gain A are shown as R_L and C_L. The external shunt capacitance C_L (typically 1 to 3 pf) is added to swamp out the stray capacitance distributed along the body of R_L. The compensation elements C_c and R_s are then added to compensate for the frequency response roll-off due to R_L and C_L. The capacitor C_s is a modification to the configuration previously published by Frodsham and Baker;[1] it is added to compensate for the roll-up associated with $C_t = C_i + C_d$, where C_i is the capacitance inherent within the preamplifier and C_d is that associated with the detector.

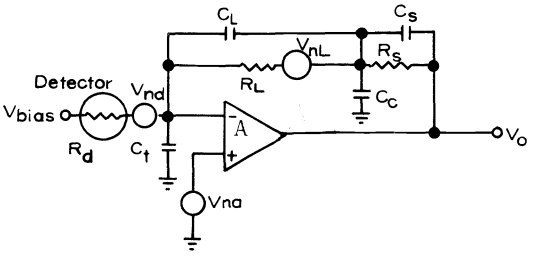

Figure 1. Configuration model for detector/preamplifier subsystem used in radiometer.

Mathematical model

The total in-band noise produced by the modeled detector/preamplifier under zilch infrared background conditions is $V_{nt} = f(R_L)f(\omega)$. The function $f(R_L)$ is given by

$$f(R_L) = R_L\{[4kTG_p + V_{na}^2 G_p^2](f_2 - f_1) + [V_{na}2\pi C_p]^2(f_2^3 - f_1^3)/3\}^{\frac{1}{2}} \quad (1)$$

where

$k = 1.38 \times 10^{-23}$ joule/°K
T = absolute temperature of R_L and R_d
f_1 = upper cut-off frequency
$G_p = 1/R_L + 1/R_d$
$C_p = C_L + C_i + C_d$

The square of the frequency function is given by

$$[f(\omega)]^2 = (\tau_s + \tau_c + 1)/\{[\tau_s + \tau_L + a\rho\tau_1/K + a\tau_d/K + \rho/K)\omega + (\tau_L\tau_{SL} - \tau_1\tau_d)\omega^3]^2 + [(1 + a\rho/K) - (\tau_s\tau_L + a\tau_1\tau_d/K + \rho\tau_1/K + \tau_d/K)\omega^2]\}^2 \quad (2)$$

where $\rho = (R_L + R_d)/R_d$ and the various time constants are given by

$\tau_s = R_sC_s$
$\tau_L = R_LC_L$
$\tau_1 = R_s(C_L + C_s)$
$\tau_d = R_L(C_L + C_d)$
$\tau_c = R_sC_c$
$\tau_{SL} = R_sC_L$

K = preamp open loop d.c. gain
a = preamp open loop frequency break point
$R_L >> R_s$
$C_s + C_c >> C_L$

Whereas the function $f(\omega)$ describes the frequency response of the model for any values of the capacitance C_s and C_c, the condition of interest is that of compensation, namely,[2]

$$C_c = R_LC_L/R_s - C_s \quad (3)$$

Under conditions of compensation, the function $f(\omega)$ simplifies to

$$f(\omega) = \omega_n^2/[\omega^2 + (2\zeta/\omega_n^2) + \omega_n^2] \quad (4)$$

where

$\omega_n = (K/R_LC_p)$
$\zeta = R_sC_s\omega_2/2$

The value of frequency ω_n is the upper cutoff frequency of the compensated detector/preamplifier combination. Therefore,

$$f_{2(max)} = (1/2\pi)[K/R_LC_p]^{\frac{1}{2}} \quad (5)$$

Under critically-damped conditions, the ζ damping factor is equal to unity. Thus, the value of C_s for the non-oscillatory case is

$$C_{s(crit)} = (2/R_s)[R_LC_p/K]^{\frac{1}{2}} \quad (6)$$

To ascertain the noise equivalent power from the model, we use the defining relationship

$$NEP = V_{n(rms)}/\text{responsivity(rms/watt)} = V_{nt}c/R_\lambda R_L T_r f(\omega) \quad (7)$$

where

c = chopping factor
T_r = transmittance
R_λ = detector current responsivity

Finally, substitution of the algorithm (Eqs. 1 and 2) for V_{nt} into Equation (7) gives

$$NEP = C/R_\lambda T_r[(4kTG_p + V_{na}{}^2G_p{}^2)(f_2 - f_1) + (V_{na}2\pi C_p)^2(f_2{}^3 - f_1{}^3)/3]^{\frac{1}{2}} \quad (8)$$

Two additional characterizing functions, which can be derived from Equations (1) and (2), are preamplifier dynamic range D_r and preamplifier output noise density $V_{na}(f)$. The dynamic range is defined as the maximum possible rms signal output voltage divided by the zero signal rms noise. Thus, a working value for D_r is simply

$$D_r = 4/f(R_L) \quad (9)$$

The noise density function $V_{nt}(f)$ expressed in volts/$\sqrt{Hz}$ is derived from V_{nt} by substituting $f = f_1 = f_2 - 1$ and $\omega/2\pi$ into Equations (1) and (2) to obtain

$$V_{nt}(f) = R_L[4kTG_p + V_{na}{}^2G_p{}^2 + (V_{na}2\pi C_p)^2(f^2 - f + 1/3)]^{\frac{1}{2}}f(\omega) \quad (10)$$

Application to radiometer

To demonstrate the utility of the computer-aided design approach, an actual application used in the design of a cryogenically-cooled, dual-channel radiometer is summarized. This radiometer was subsequently flown on a space vehicle.

Equations (1) through (10) characterize the Frodsham-Baker detector/preamplifier model for any given detector assuming the detector resistance R_d and capacitance C_c are known. In Table 1 below, these detector parameters are characterized as a function of sensitive area for three types of detectors: (1) intrinsic silicon at 77°K, (2) extrinsic silicon at 10°K, and (3) indium antimonide at 77°K.

Table 1. Detector characteristics

R_d(ext. Si) $\simeq 1.35 \times 10^{12}/A_d$	(ohms)
C_d(ext. Si) $\simeq 2 \times 10^{-13}[A_d]$	(farads)
R_d(int. Si) $\simeq 1 \times 10^{15}$	(ohms)
C_d(int. Si) $\simeq 1 \times 10^{-11}[A_d]^{\frac{1}{2}}$	(farads)
R_d(InSb) $\simeq 2 \times 10^6/A_d$	(ohms)
C_d(InSb) $\simeq 5 \times 10^{-8} \cdot A_d$	(farads)

where A_d = detector active area

The system design parameters for the dual-channel radiometer, which is liquid-nitrogen cooled and is designated by the Model No. NR-7, are listed in Table 2 (computer listing).

Table 2. The system input parameters are:

```
Signal Coupling (AC or DC)-(F$)= AC
Electrical Bandwidth-------(F3)= 3.ØØE+ØØ1(HZ)
Chopper Frequency----------(F4)= 1.ØØE+ØØ2(HZ)
Preamp Input Capacitance---(A1)= 8.ØØE-Ø12(FARAD)
Preamp Input Noise---------(A2)= 2.ØØE-ØØ8(V/√HZ)
Feedback Resistance--------(A3)= 1.ØØE+ØØ9(OHMS)
Feedback Capacitance-------(A4)= 1.ØØE-Ø12(FARADS)
Component Temperature------(A5)= 7.7ØE+ØØ1(KELVIN)
Detector Area--------------(D1)= 7.85E-ØØ3(SQ.CM)
Detector Responsivity------(D2)= 1.ØØE+ØØØ(A/W)
Det. Type(In:Sb,As:Si,Si1) (D$)= In:Sb
Collector Area-------------(01)= 1.82E+ØØØ(SQ.CM)
Field of View(Half Angle)--(02)= 2.ØØE+ØØØ(DEG)
Optical Transmission-------(03)= 3.5ØE-ØØ1
```

The parameter values shown for the chopper frequency, the resistance and capacitance, and the detector area are initial estimates for the working values. The final design values, along with those for the compensation elements, were determined by the computer-aided design approach as follows.

The feedback load resistance R_L was determined from the computer-generated curve shown as Figure 2. The value was selected as 10^9 ohms since this gave an NEP which was less than half of a decibel more than would occur for an infinite value for R_L (indicated as zero db on the ordinate scale) without impacting the dynamic range specification of 10^5 nor the upper frequency cutoff requirement of 130 Hz.

Next, the detector area was examined with the aid of the generated curves shown in Figure 3. Since the optimum value of the load resistance (recomputed for each value of detector area) decreases as A_d increases, the resultant NEP value worsens as the area increases. Consequently, the dynamic range capability also increases with increased detector size. It can be seen from the curves that the NER is approaching a constant and is less than 3 db above the asymptotic value at the preselected value of $7.85 \times 10^{-3} cm^2$ for area.

From the curve shown in Figure 4, the effect of changing the chopping frequency can be analyzed. The practical application of the Nyquist rate dictates that the chopper frequency be at least the 100 Hz initially selected. Any increase above the selected value of 100 Hz would cause a degredation of both the dynamic range and the NEP.

Figure 5 gives the computed frequency curve for the detector/preamplifier combination for Channel A of the radiometer using the actual and/or initially estimated parameter values as shown. Curve 1 is the desired frequency response. Using the initially selected values of 27 and 56 pf for C_S and C_C, respectively, the frequency response curve was then experimentally measured. The unsatisfactory result is shown as Curve 1 in Figure 6. Using this curve, the computer model parameters were adjusted to reproduce the unsatisfactory response curve; the values of C_S and C_C given by the computer were 24 and 42 pf, respectively. The next step was to ratio the two sets of values, giving a value set of 30 and 75 pf. The final step was to experimentally measure the response curve again using these new values. The result is Curve 2 of Figure 6 which shows excellent agreement with the frequency response desired.

Figures 7 and 8 show the similar computer-aided analyses applied to Channel B of the radiometer. In this case a slightly larger value of C_L was selected initially; the result was the computer curve of Figure 7. The measured response curve, given in Figure 8, shows excellent agreement without changing the compensation element values. Finally, the detector/preamplifier noise density functions (volts/√Hz) were computed for both Channels A and B. The results are shown in Figures 9 and 10, respectively. These data were generated to verify preamplifier performance by comparing with measured data, and in this case good agreement was found.

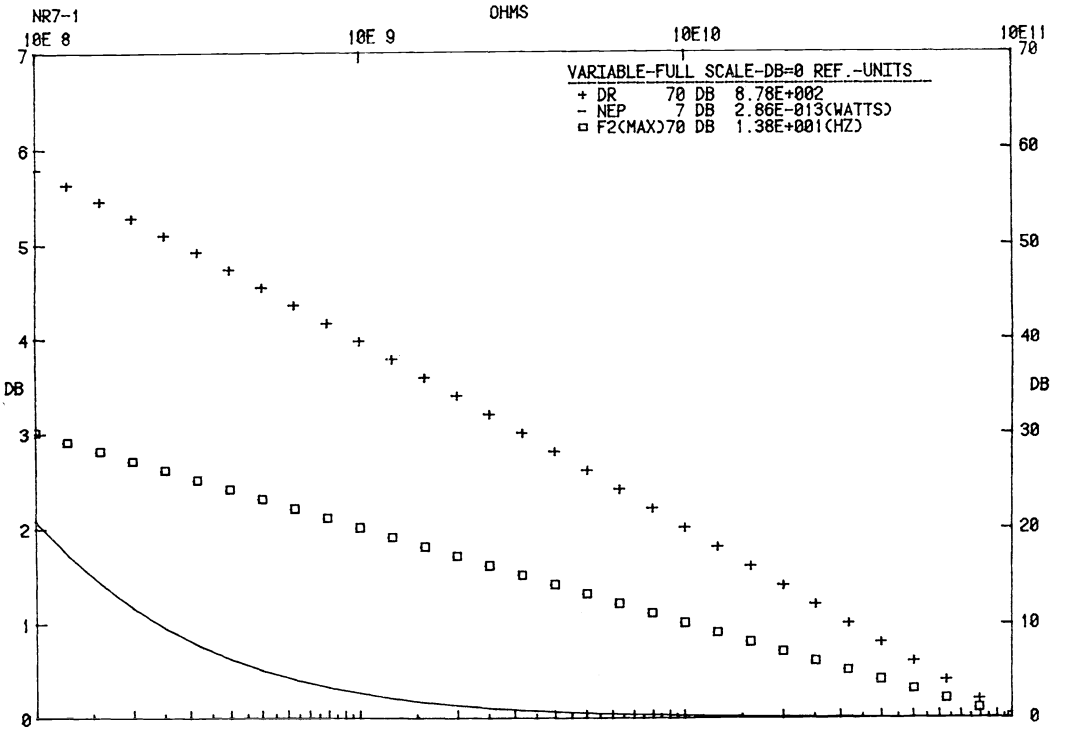

Figure 2. Relative dynamic range, NEP and upper frequency cutoff as a function of R_L.

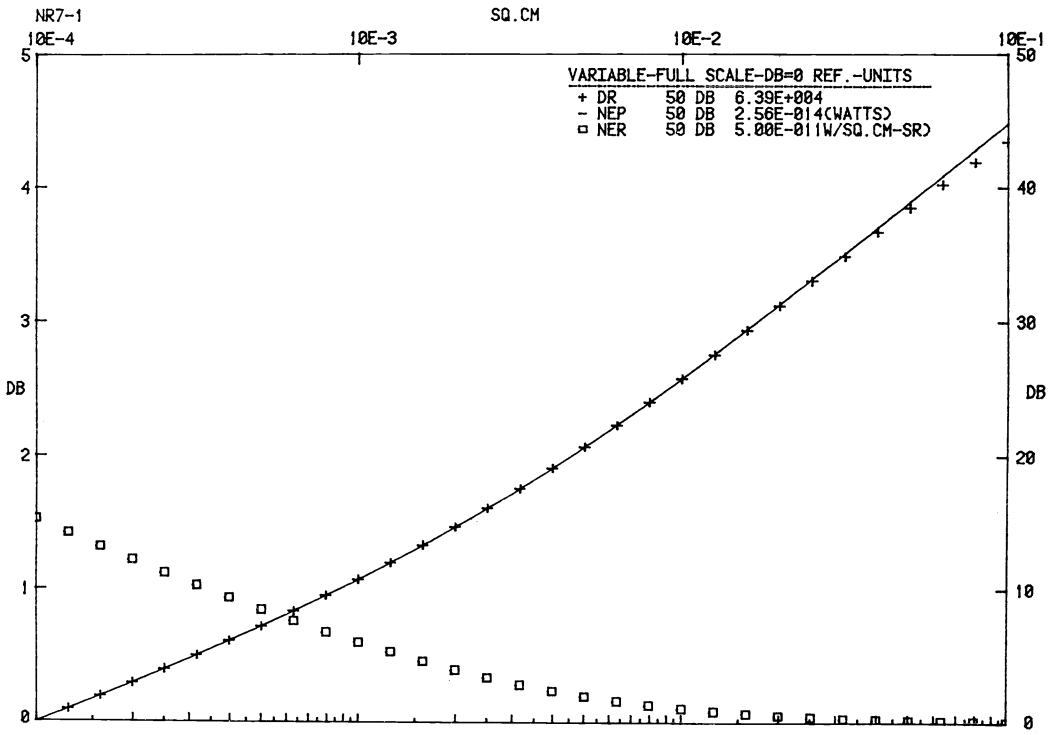

Figure 3. Dynamic range, NEP and NER as a function of detector area A_d.

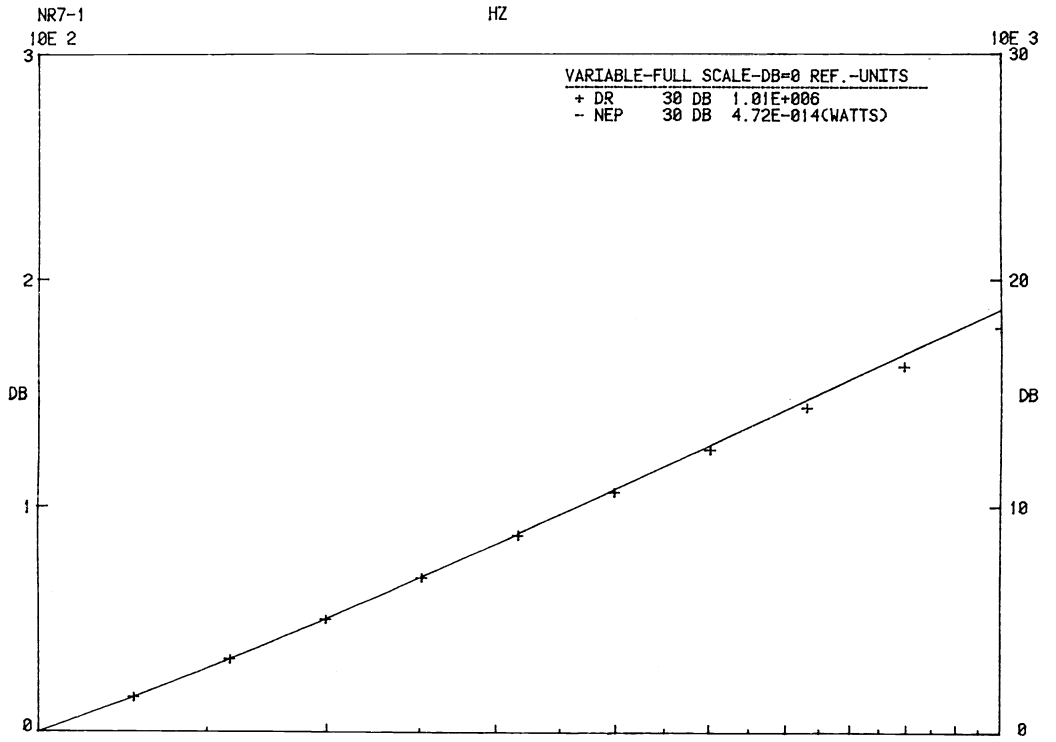

Figure 4. Dynamic range and NEP as a function of chopping frequency f.

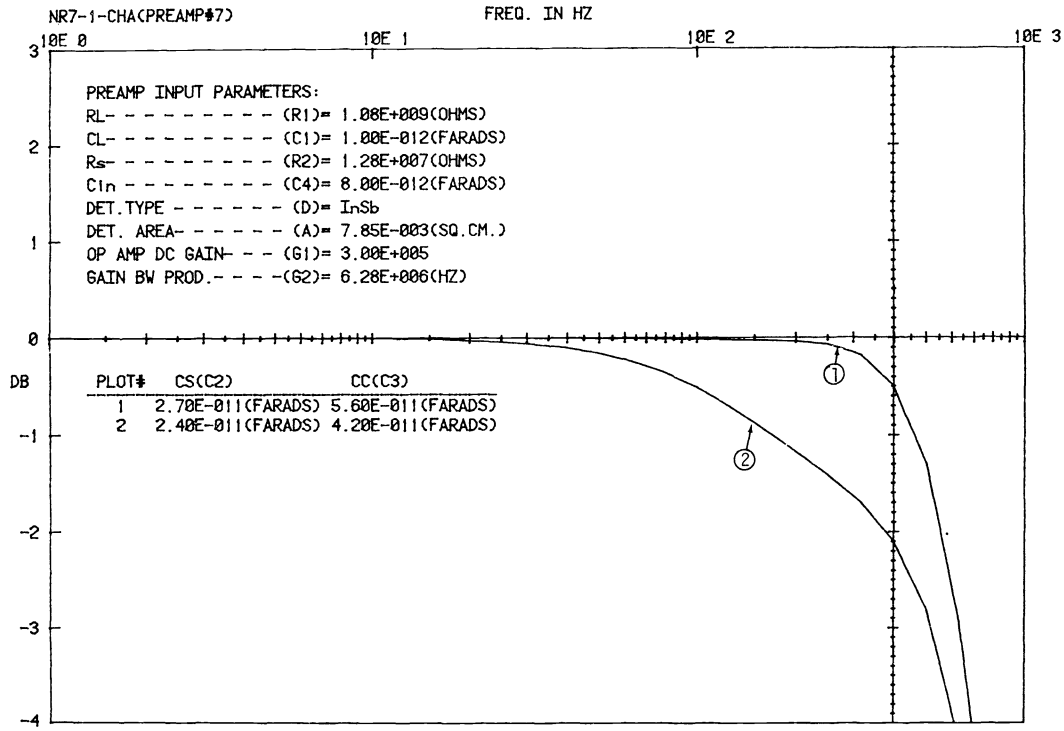

Figure 5. Computed relative frequency response for two sets of values of compensation capacitors C_s and C_c for Channel A detector/preamplifier.

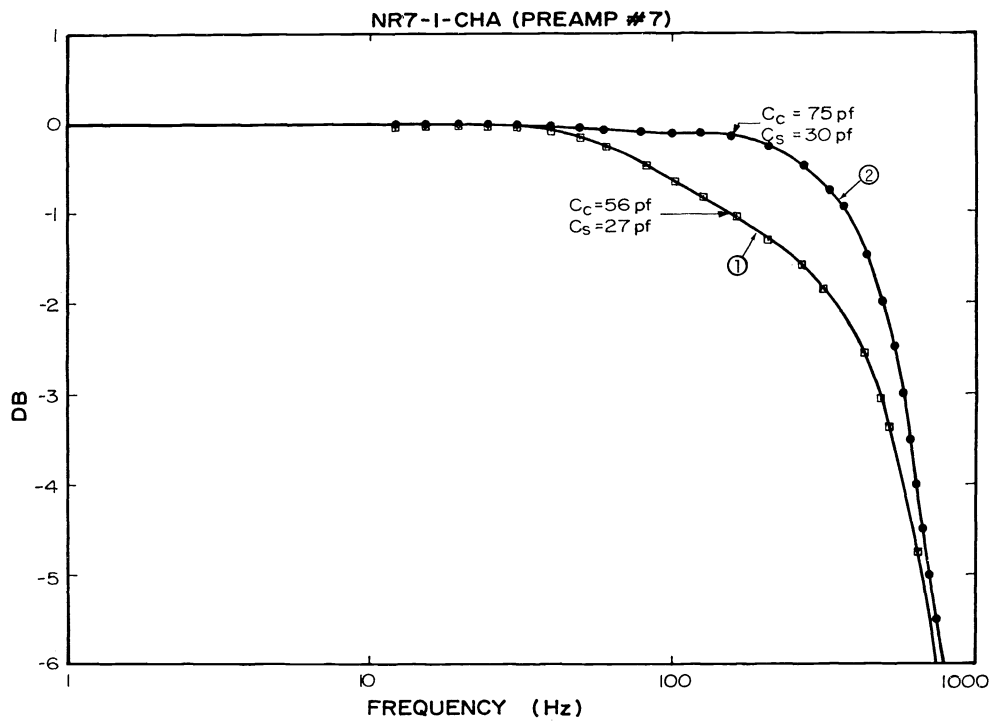

Figure 6. Measured relative frequency response for initial and final sets of values for C_s and C_c for Channel A detector/preamplifier.

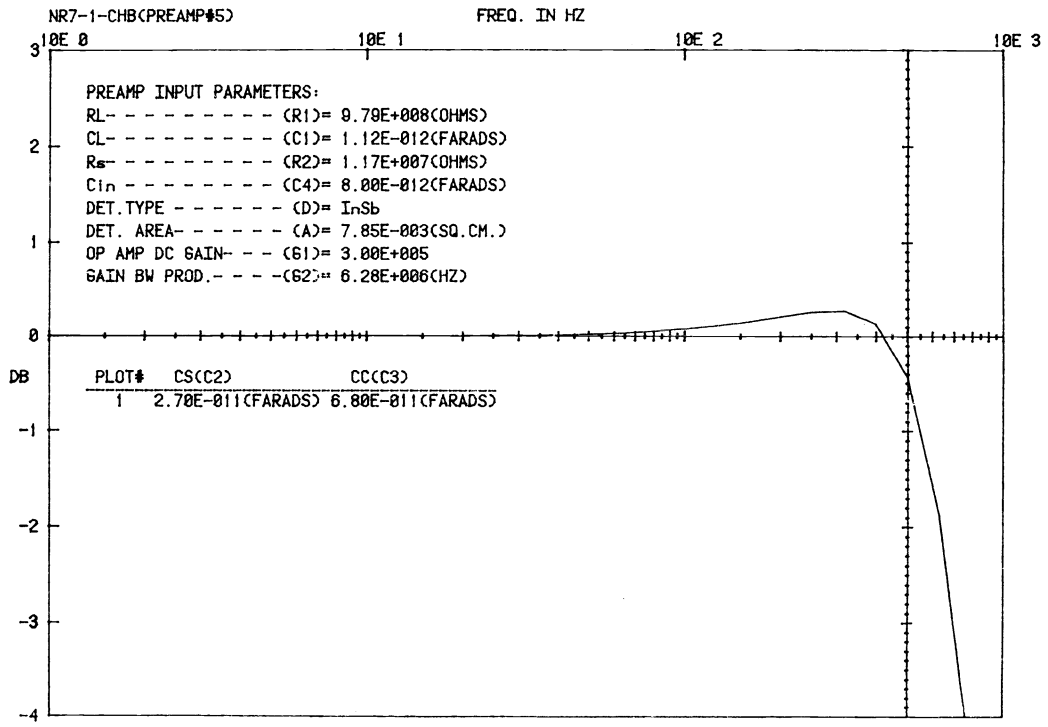

Figure 7. Computed frequency response for Channel B detector/preamplifier.

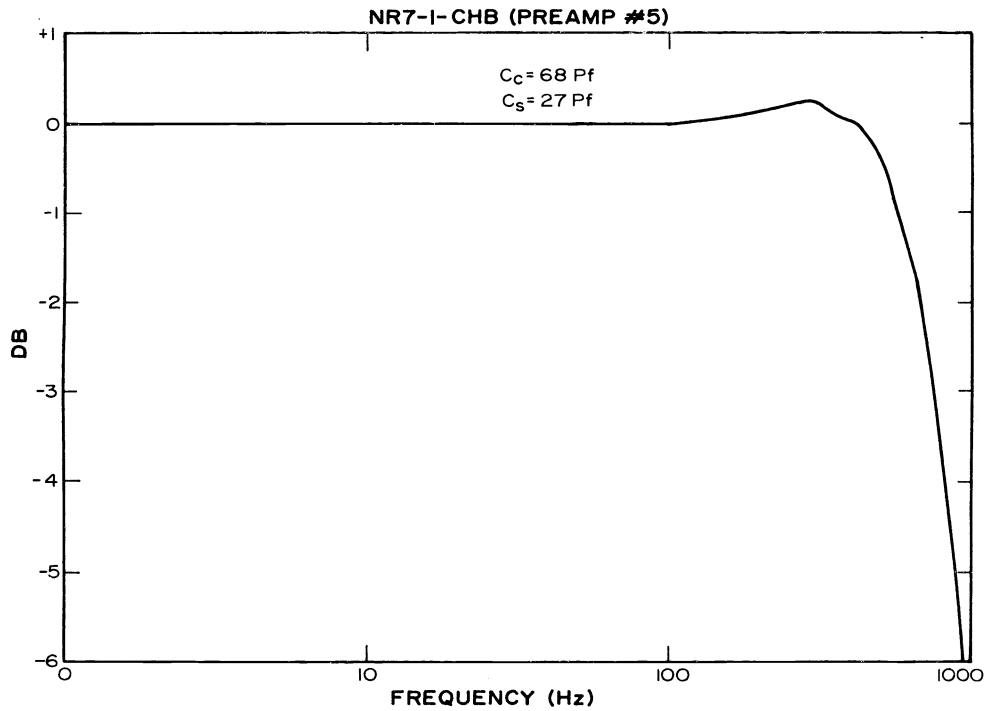

Figure 8. Measured response for Channel B detector/preamplifier.

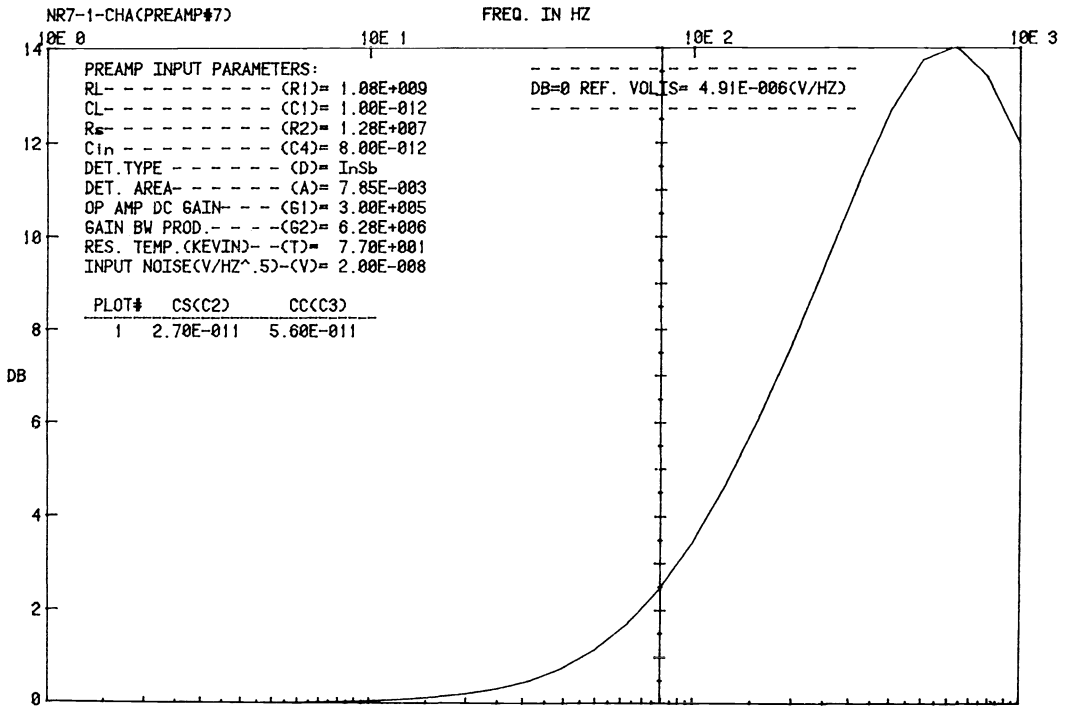

Figure 9. Computed preamplifier output noise density $V_{nt}(f)$ versus frequency for Channel A detector/preamplifier.

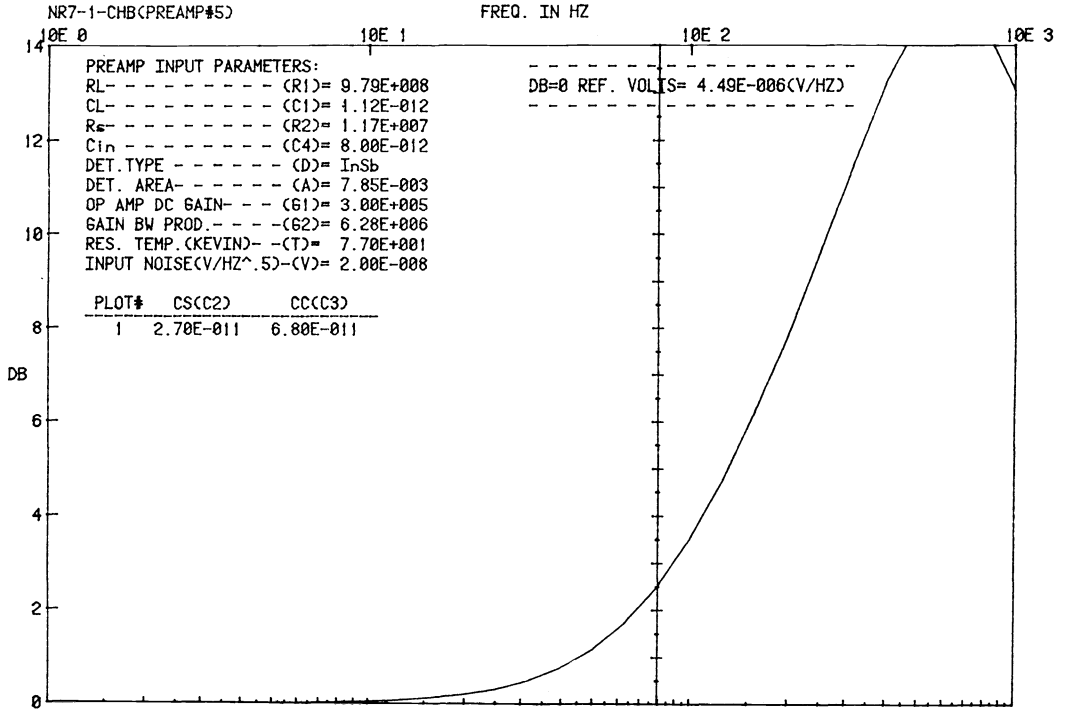

Figure 10. Computed preamplifier output noise density $V_{nt}(f)$ versus frequency for Channel B detector/preamplifier.

References

1. Frodsham, D. G. and D. J. Baker, "Optimization of Detector-Preamplifier for Cryogenic Spectrometry," *Proc. Soc. Photo Optical Instrumentation Engineers*, Vol. 191, pp. 130-134. August 27-28, 1979.

2. Baker, D. J., C. L. Wyatt, and F. R. Brown, Jr., "A Direct-Coupled DC Amplifier Compensated to 20 KC for Use with Photoemissive Devices," *IEEE Trans. on Instrumentation and Measurement*, Vol. IM-13, Nos. 2 & 3, pp. 115-118. June-September 1964.

Acknowledgments

The authors hereby express appreciation to our colleagues who have provided assistance in both the preparation of this specific paper and in the general infrared systems area research project which was sponsored by the Air Force Geophysics Laboratory. Among these individuals are Al McIntire, A.T. Stair, Jr., Gene Ware, Lynn Bates, and Allan Steed.